

Novel MAB phases and insights into their exfoliation into 2D MBenes

Mohammad Khazaei,¹ Junjie Wang,^{2,3} Mehdi Estili,⁴ Ahmad Ranjbar,¹
Shigeru Suehara,⁵ Masao Arai,⁵ Keivan Esfarjani,⁶ and Seiji Yunoki^{1,7,8}

¹Computational Materials Science Research Team, RIKEN Center for Computational Science (R-CCS), Kobe, Hyogo 650-0047, Japan

²State Key Laboratory of Solidification Processing, Northwestern Polytechnical University, Xi'an, Shaanxi 710072, People's Republic of China

³International Center for Materials Discovery, School of Materials Science and Engineering,
Northwestern Polytechnical University, Xi'an, Shaanxi 710072, People's Republic of China

⁴Research Center for Functional Materials (RCFM), National Institute for Materials Science (NIMS), Tsukuba 305-0047, Japan

⁵International Center for Materials Nanoarchitectonics,

National Institute for Materials Science (NIMS), 1-1 Namiki, Tsukuba 305-0044, Ibaraki, Japan

⁶Departments of Mechanical and Aerospace Engineering, Physics, and Materials Science and Engineering,
University of Virginia, 122 Engineer's Way, Charlottesville, VA 22904, USA

⁷Computational Condensed Matter Physics Laboratory,

RIKEN Cluster for Pioneering Research (CPR), Wako, Saitama 351-0198, Japan

⁸Computational Quantum Matter Research Team, RIKEN Center for Emergent Matter Science (CEMS), Wako, Saitama 351-0198, Japan

(Dated: May 20, 2019)

Considering the recent breakthroughs in the synthesis of novel two-dimensional (2D) materials from layered bulk structures, ternary layered transition metal borides, known as MAB phases, have come under scrutiny as a means of obtaining novel 2D transition metal borides, so-called MBene. Here, based on a set of phonon calculations, we show the dynamic stability of many Al-containing MAB phases, MAIB ($M = \text{Ti, Hf, V, Nb, Ta, Cr, Mo, W, Mn, Tc}$), $M_2\text{AlB}_2$ ($M = \text{Sc, Ti, Zr, Hf, V, Cr, Mo, W, Mn, Tc, Fe, Rh, Ni}$), $M_3\text{Al}_2\text{B}_2$ ($M = \text{Sc, Ti, Zr, Hf, Cr, Mn, Tc, Fe, Ru, Ni}$), $M_3\text{AlB}_4$ ($M = \text{Sc, Ti, Zr, Hf, V, Nb, Ta, Cr, Mo, W, Mn, Fe}$), and $M_4\text{AlB}_6$ ($M = \text{Sc, Ti, Zr, Hf, V, Nb, Ta, Cr, Mo}$). By comparing the formation energies of these MAB phases with those of their available competing binary M–B and M–Al, and ternary M–Al–B phases, we find that some of the Sc-, Ti-, V-, Cr-, Mo-, W-, Mn-, Tc-, and Fe-based MAB phases could be favorably synthesized in an appropriate experimental condition. In addition, by examining the strengths of various bonds in MAB phases via crystal orbital Hamilton population and spring constant calculations, we find that the B–B and then M–B bonds are stiffer than the M–Al and Al–B bonds. The different strength between these bonds implies the etching possibility of Al atoms from MAB phases, consequently forming various 2D MB, M_2B_3 , and M_3B_4 MBenes. Furthermore, we employ the nudged elastic band method to investigate the possibility of the structural phase transformation of the 2D MB MBenes into graphene-like boron sheets sandwiched between transition metals and find that the energy barrier of the transformation is less than 0.4 eV/atom.

INTRODUCTION

The possibility of chemical exfoliation of layered bulk structures has brought great hope to synthesis novel 2D materials with unique electronic and mechanical properties in the future. In this regard, many members of the family of layered transition metal carbides and nitrides, known as MAX phases,^[1–3] have been exfoliated into 2D transition metal carbides. ^[4, 5] MAX phases have a general chemical formula of $M_n\text{AX}_{n+1}$, where M is a transition metal (Sc, Ti, Zr, Hf, V, Nb, Ta, Cr, and Mo), A is an element from groups IIIA–VIA in the periodic table (*i.e.*, Al, Ga, Si, Ge, Sn, Pb, P, As, Bi, S, Se, and Te), and X stands for carbon/nitrogen.^[1–3] Recently, more complex MAX phases with ordered double transition metals have also been developed.^[6–8] In MAX phases, generally, the strength of M–A bonds are relatively weaker than the M–X bonds.^[9] Such bond strength characteristics make it possible to break the M–A bonds using appropriate chemical solutions while M–X bonds remain almost intact.^[9] In other words, by the chemical treatment, the “A” atoms are washed out from the MAX phases while the backbones, *i.e.*, the multilayers of 2D $M_n\text{X}_{n+1}$, remains stable. By ultrasonication, the multilayers can be separated into monolayers, named as MXenes. ^[4, 5] For examples, Ti_2AlC , Ti_2AlN , V_2AlC , Nb_2AlC , Ti_3AlC_2 , Ti_3SiC_2 , Ti_4AlN_3 , V_4AlC_3 , Nb_4AlC_3 , Ta_4AlC_3 ,

$\text{Mo}_2\text{ScAlC}_2$, $\text{Mo}_2\text{TiAlC}_2$, $\text{Mo}_2\text{Ti}_2\text{AlC}_3$, $(\text{Mo}_{2/3}\text{Sc}_{1/3})_2\text{AlC}$, $(\text{W}_{2/3}\text{Y}_{1/3})_2\text{AlC}$, and many others have already been exfoliated into their corresponding 2D MXenes.^[4–8, 10–15] Additionally, the above chemical technique has been successfully applied to exfoliate non-MAX phase structures such as ScAl_3C_3 , $\text{Mo}_2\text{Ga}_2\text{C}$, $\text{Zr}_3\text{Al}_3\text{C}_5$, and $\text{Hf}_3\text{Al}_4\text{C}_6$ to obtain 2D ScC_x , Mo_2C , Zr_3C_2 , and Hf_3C_2 , respectively.^[16–19] More recently, MoAlB with double Al layers, a member of transition metal boride phases, known as MAB phases, has also been partially etched into 2D MoB .^[20, 21] Also 2D CrB was obtained from chemical exfoliation of MAB phase Cr_2AlB_2 .^[22, 23] In analogous to the MAX phases, where after etching the “A” elements their corresponding 2D materials were named as MXenes, the 2D transition metal borides, which are obtained by etching the “A” elements from the MAB phases, are called MBenes. It is noteworthy that the electronic and magnetic applications of 2D transition metal borides are growing very fast. ^[24–28] Recent calculations indicate that 2D MBenes may have applications for Li- and Na-ion batteries,^[29, 30] electrocatalysis,^[20, 29] and magnetic ^[31] devices. Similar to 2D MXenes,^[32–45] it is expected MBenes may find many potential applications in electronic, optoelectronic, and energy devices in the future.

As listed above, many Al-containing MAX phases have already been exfoliated into 2D MXenes. This motivated ex-

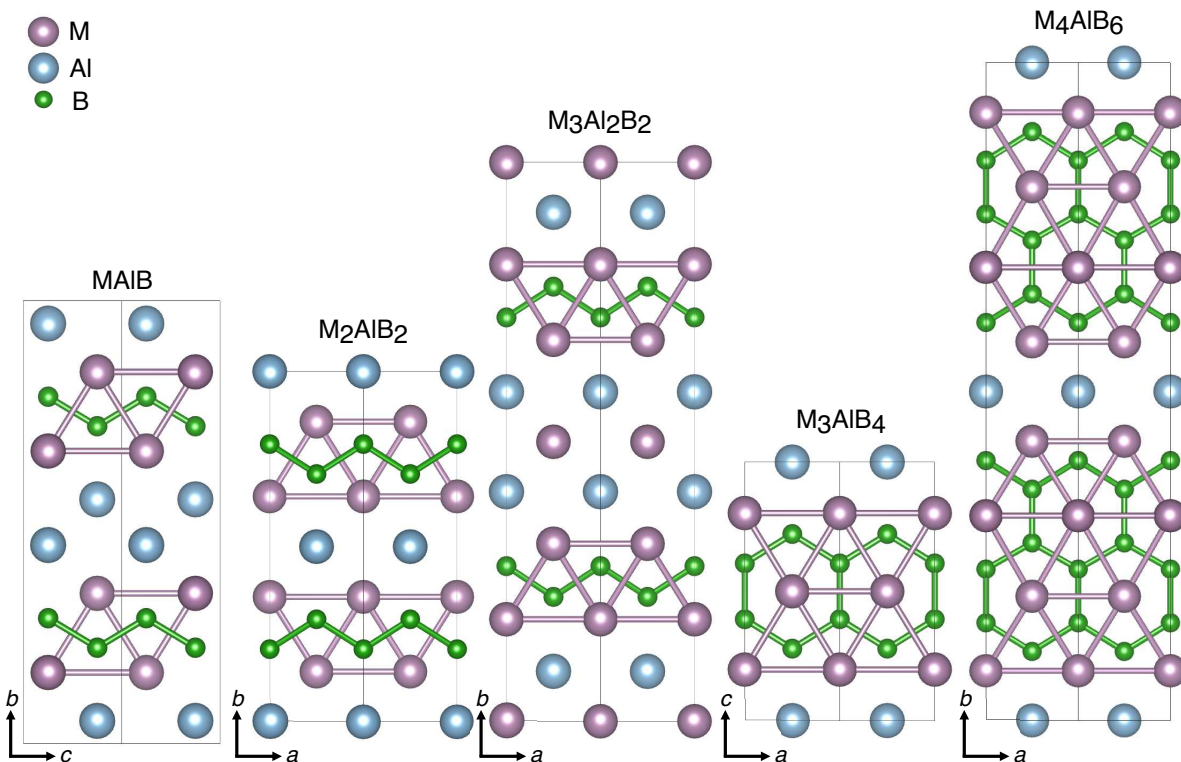


FIG. 1. Crystal structures of various MAB phases. M, Al and B atoms are denoted by purple, blue, and green spheres, respectively. a , b , and c directions are indicated by arrows.

perimentalists to focus on the Al-containing MAB phases as promising candidates for obtaining new 2D transition metal borides. MAB phases are orthorhombic crystals with the chemical formula of MAIB, M₂AlB₂, M₃Al₂B₂, M₃AlB₄, and M₄AlB₆, shown in Figure 1. Experimentally, MAIB (M = Mo and W), M₂AlB₂ (M = Cr, Mn, and Fe), Ru₃Al₂B₂, Cr₃AlB₄, and Cr₄AlB₆ have already been synthesized.[22, 23, 46–53] As seen from Figure 1, the skeleton of MAIB, M₂AlB₂, and M₃Al₂B₂ contains isolated zigzag chains of boron atoms, while M₃AlB₄ and M₄AlB₆ contain double and triple chains of boron atoms, respectively, connected to form flat strips with hexagonal boron ring networks. In this paper, we extend the family members of MAB phases by studying the dynamic stability and the formation energy of MAIB, M₂AlB₂, M₃Al₂B₂, M₃AlB₄, and M₄AlB₆ (M = Sc, Ti, Zr, Hf, V, Nb, Ta, Cr, Mo, W, Mn, Tc, Fe, Ru, Co, Rh, and Ni). In excellent agreement with experiments, our formation energy calculations indicate that some of the Cr-, Mo-, W-, Mn-, and Fe-based MAB phases can be formed experimentally. Although Sc-, Ti-, and V-based MAB phases are slightly metastable compared to the most stable MAB phases described above, they have a high probability of being formed experimentally. Bond strength calculations indicate that B–B and M–B are stiffer than the M–Al and Al–B bonds, which indicates the possibility of etching the Al atoms from MAB phases and thus forming 2D MBenes. Furthermore, using the nudged elastic band method, we investigate the possibility of the rearrangement of boron chains in 2D MB MBene into a 2D graphene-like boron sheet

that is sandwiched between the metal layers. This process results in structural phase transformation of the 2D MB MBene with rectangular lattice to a hexagonal lattice. The same transformation process may occur in M₂B₃ and M₃B₄ MBenes, resulting in the formation of double and triple graphene-like boron sheets sandwiched between the metal layers.

I. METHODS OF CALCULATIONS

First-principles calculations based on density functional theory (DFT) are performed to optimize the atomic structures and examine the electronic structures of the MAB phases. All calculations are carried out using the Vienna ab initio simulation package (VASP) code.[54] The generalized gradient approximation (GGA) using the Perdew-Burke-Ernzerhof (PBE) functional is used to compute the exchange-correlation energy.[55] The projected augmented wave approach with a plane wave cutoff energy of 520 eV is used to construct the wave functions. The atomic positions and lattice constants are fully optimized using the conjugate gradient method without imposing any symmetry. After the optimization of atomic structures, the maximum residual force on each atom is less than 0.001 eV/Å. In the electronic self-consistency procedure, the total energies are converged within 10⁻⁷ eV/cell. For the optimization of MAIB, M₂AlB₂, M₃Al₂B₂, and M₄AlB₆ (M₃AlB₄), 18×9×18 (18×18×9) Monkhorst-Pack \mathbf{k} points are used.[56] Most of the MAB phases are nonmagnetic, except

TABLE I. List of MAB phases that we found dynamically stable based on phonon calculations. a , b , and c are the lattice parameters. ΔH indicates the instability energy of MAB phases over competing phases. FC_M , FC_{Al} , FC_B , are total force constants on M, Al, and B atoms, respectively. E_{ext} is the static exfoliation energy. The MAB phases experimentally synthesized are indicated by asterisks (\star). The experimental lattice parameters of the MAB phases already synthesized are also listed in parentheses.

MAB phase	a (Å)	b (Å)	c (Å)	Most competing phases	ΔH (eV/atom)	FC_M (eV/Å ²)	FC_{Al} (eV/Å ²)	FC_B (eV/Å ²)	E_{ext} (eV/Å ²)
TiAlB	3.285	14.661	3.055	TiAl ₂ , TiB ₂	0.126	44.830	18.707	44.224	0.142
HfAlB	3.455	15.516	3.155	HfB ₂ , HfAl ₂	0.176	46.223	15.127	40.700	0.125
VAIB	3.091	14.201	3.005	V ₃ B ₄ , VAl ₃ , Al	0.041	48.964	26.237	45.971	0.187
NbAlB	3.343	14.714	3.130	NbAl ₃ , Nb ₃ B ₄ , NbB ₂	0.090	51.156	21.889	38.443	0.176
TaAlB	3.330	14.638	3.107	Ta ₃ B ₄ , Al, TaAl ₃	0.055	53.138	24.064	40.307	0.187
CrAlB	3.003	13.889	2.969	Cr ₂ AlB ₂ , Al	0.008	50.379	31.043	48.607	-0.205
MoAlB \star [48]	3.216 (3.199 [48])	14.025 (13.922 [48])	3.110 (3.094 [48])	MoB, MoB ₂ , Mo ₃ Al ₈	-0.114	56.367	29.542	39.139	0.225
WAlB \star [48]	3.220 (3.202 [48])	13.976 (13.906 [48])	3.118 (3.102 [48])	WB ₂ , WB, WAl ₅	-0.022	57.306	31.878	39.098	0.229
MnAlB	2.955	13.859	2.989	MnAl ₆ , Mn ₂ AlB ₂ , MnB ₄	0.065	34.122	29.090	46.380	0.159
TcAlB	3.025	14.099	3.168	TcAl ₃ , Tc ₂ Al, TcB ₂	0.015	38.686	31.604	34.388	0.203
Sc ₂ AlB ₂	3.178	11.724	3.614	ScAl, ScB ₂	0.041	33.538	20.963	34.806	0.095
Ti ₂ AlB ₂	3.047	11.323	3.311	Ti ₃ B ₄ , TiB ₂ , TiAl	0.026	43.162	25.248	44.433	0.149
Zr ₂ AlB ₂	3.192	12.012	3.605	ZrB ₂ , Zr ₂ Al ₃ , Zr ₄ Al ₃	0.080	43.720	21.206	36.494	0.115
Hf ₂ AlB ₂	3.166	11.799	3.553	Hf ₄ Al ₃ , HfB ₂ , HfAl ₂	0.078	46.087	23.137	38.012	0.129
V ₂ AlB ₂	3.012	11.109	3.075	VB, V ₃ B ₄ , VAl ₃	0.097	47.491	25.784	45.554	0.174
Cr ₂ AlB ₂ \star [48]	2.924 (2.937 [48])	11.051 (11.051 [48])	2.934 (2.967 [48])	Cr ₃ AlB ₄ , Cr ₇ Al ₄₅ , CrB	-0.044	58.667	29.668	49.742	0.216
Mo ₂ AlB ₂	3.076	11.543	3.146	MoB, MoAlB	0.012	59.637	24.739	39.849	0.210
W ₂ AlB ₂	3.085	11.584	3.138	WB ₂ , WB, WAl ₅	0.039	63.566	26.312	40.231	0.215
Mn ₂ AlB ₂ \star [48]	2.896 (2.918[48])	11.074 (11.038[48])	2.831 (2.893[48])	Mn ₄ Al ₁₁ , MnB, MnB ₄	-0.060	45.586	31.649	49.062	0.193
Tc ₂ AlB ₂	3.043	11.576	3.018	TcAl ₃ , Tc ₂ Al, TcB ₂	-0.050	48.192	28.249	38.614	0.217
Fe ₂ AlB ₂ \star [48]	2.917 (2.922[48])	11.024 (10.991[48])	2.853 (2.856[48])	FeAl ₆ , TiB ₂ , FeB	-0.078	37.618	28.990	45.971	0.181
Ru ₃ AlB ₂	2.955	12.849	2.829	RuB ₂ , Ru ₄ Al ₃ B ₂	0.107	42.628	19.776	37.506	0.205
Rh ₂ AlB ₂	3.103	12.253	2.860	RhAl, RhB, B	0.263	19.849	18.892	29.707	0.134
Ni ₂ AlB ₂	2.980	11.051	2.850	Ni ₁₂ AlB ₈ , B, NiAl	0.139	19.596	25.579	38.699	0.115
Sc ₃ Al ₂ B ₂	3.192	18.385	3.600	ScAl, ScB ₂	0.024	33.835	20.169	34.116	0.135
Zr ₃ Al ₂ B ₂	3.180	18.335	3.691	ZrB ₂ , Zr ₂ Al ₃ , Zr ₄ Al ₃	0.098	41.153	20.197	35.366	0.143
Hf ₃ Al ₂ B ₂	3.150	18.073	3.638	Hf ₄ Al ₃ , HfB ₂ , HfAl ₂	0.100	43.180	21.860	36.989	0.149
Cr ₃ Al ₂ B ₂	2.936	17.313	2.951	Cr ₂ AlB ₂ , CrAl ₃ , Cr ₂ Al	0.038	53.461	26.445	48.447	0.213
Mn ₃ Al ₂ B ₂	2.851	17.863	2.833	MnAl, Mn ₂ AlB ₂	0.004	49.480	26.209	50.172	0.228
Tc ₃ Al ₂ B ₂	3.045	17.545	3.054	TcAl ₃ , Tc ₂ Al, TcB ₂	-0.037	48.663	26.422	37.386	0.255
Fe ₃ Al ₂ B ₂	2.913	16.536	2.875	Fe ₂ AlB ₂ , FeAl	-0.013	35.806	30.439	45.163	0.225
Ru ₃ Al ₂ B ₂ \star [46]	3.045 (2.967[46])	17.824 (17.036[46])	2.938 (2.965[46])	RuB ₂ , Ru ₄ Al ₃ B ₂	0.070	33.390	28.486	32.482	0.277
Ni ₃ Al ₂ B ₂	2.962	16.926	2.840	Ni ₁₂ AlB ₈ , B, NiAl	0.084	20.469	25.573	38.568	0.202
Sc ₃ AlB ₄	3.157	3.565	8.630	ScAl, ScB ₂	0.035	34.006	21.866	35.629	0.100
Ti ₃ AlB ₄	3.039	3.296	8.254	Ti ₃ B ₄ , TiB ₂ , TiAl	0.040	44.608	26.571	44.955	0.152
Zr ₃ AlB ₄	3.187	3.595	8.711	ZrB ₂ , Zr ₂ Al ₃ , Zr ₄ Al ₃	0.052	45.443	22.684	36.802	0.125
Hf ₃ AlB ₄	3.155	3.534	8.608	Hf ₄ Al ₃ , HfB ₂ , HfAl ₂	0.073	47.672	24.291	39.102	0.137
V ₃ AlB ₄	2.976	3.059	8.191	V ₃ B ₄ , VAl ₃ , Al	0.046	50.634	25.465	47.017	0.195
Nb ₃ AlB ₄	3.126	3.314	8.609	NbAl ₃ , Nb ₃ B ₄ , NbB ₂	0.087	49.773	20.258	38.349	0.171
Ta ₃ AlB ₄	3.110	3.304	8.544	Ta ₃ B ₄ , Al, TaAl ₃	0.092	50.945	21.925	39.526	0.179
Cr ₃ AlB ₄ \star [48]	2.939 (2.956[48])	2.939 (2.978[48])	8.088 (8.054[48])	Cr ₂ AlB ₂ , CrB, CrB ₄	-0.004	57.605	30.273	48.514	0.209
Mo ₃ AlB ₄	3.087	3.168	8.395	MoB, MoB ₂ , MoAlB	-0.027	58.688	25.948	38.797	0.196
W ₃ AlB ₄	3.093	3.177	8.381	WB ₂ , WB, WAl ₅	0.084	60.745	28.368	38.852	0.170
Mn ₃ AlB ₄	2.937	2.835	8.153	MnB, Mn ₂ AlB ₂ , MnB ₄	0.036	45.581	30.902	46.191	0.190
Fe ₃ AlB ₄	2.960	2.819	8.144	Fe ₂ AlB ₂ , FeB, B	0.063	33.713	28.099	42.178	0.163
Sc ₄ AlB ₆	3.154	22.721	3.551	ScAl, ScB ₂ , Sc ₂ Al	0.028	34.172	21.600	35.482	0.099
Ti ₄ AlB ₆	3.035	21.840	3.267	Ti ₃ B ₄ , TiB ₂ , TiAl	0.036	44.752	26.494	44.963	0.156
Zr ₄ AlB ₆	3.182	22.999	3.575	ZrB ₂ , Zr ₂ Al ₃ , Zr ₄ Al ₃	0.059	45.655	22.318	36.810	0.128
Hf ₄ AlB ₆	3.150	22.731	3.511	Hf ₄ Al ₃ , HfB ₂ , HfAl ₂	0.061	47.867	23.789	39.083	0.141
V ₄ AlB ₆	2.973	21.617	3.050	V ₂ B ₃ , Al	0.026	53.266	25.311	47.074	0.198
Nb ₄ AlB ₆	3.118	22.604	3.328	NbAl ₃ , Nb ₃ B ₄ , NbB ₂	0.057	53.062	20.864	38.425	0.168
Ta ₄ AlB ₆	3.099	22.511	3.312	TaB ₂ , Ta ₃ B ₄ , Al	0.049	55.537	22.365	39.789	0.178
Cr ₄ AlB ₆ \star [48]	2.947 (2.952[48])	21.325 (21.280[48])	2.944 (3.013[48])	CrB ₄ , Cr ₃ AlB ₄ , CrB	0.008	57.827	30.251	48.589	0.200
Mo ₄ AlB ₆	3.080	22.091	3.195	MoB, MoB ₂ , MoAlB	-0.021	58.159	25.808	38.828	0.181

for Cr-, Mn-, and Fe-based MAB phases. The total energies and properties of the magnetic MAB phases and all 2D MBenes are evaluated using spin-polarized calculations.

The phonon calculations are carried out using the PHONOPY package [57] along with the VASP.[54] To evaluate the strength of the bonds, it is assumed the atoms in a bond are connected by springs.[9] The spring or force constant is the second derivative of the total energy with respect to finite displacements of atoms i and j along the x , y , and z directions, and is described as a 3×3 matrix, which is one of the output results of the phonon calculations. Since the trace

of the force constant matrix is independent of the coordinate system, *i.e.*, invariant under a coordinate rotation,[58, 59] we consider the value of the trace of the force constant matrix and refer to this scalar quantity as the force constant F_{ij} between atoms i and j .[9, 59]

As another method for evaluating a bond strength, we also employ the crystal orbital Hamilton population (COHP) analysis.[60] The COHP analysis is a technique for partitioning the band-structure energy into bonding, nonbonding, and antibonding contributions using localized atomic basis sets.[60] It describes as a hopping-weighted density-of-states

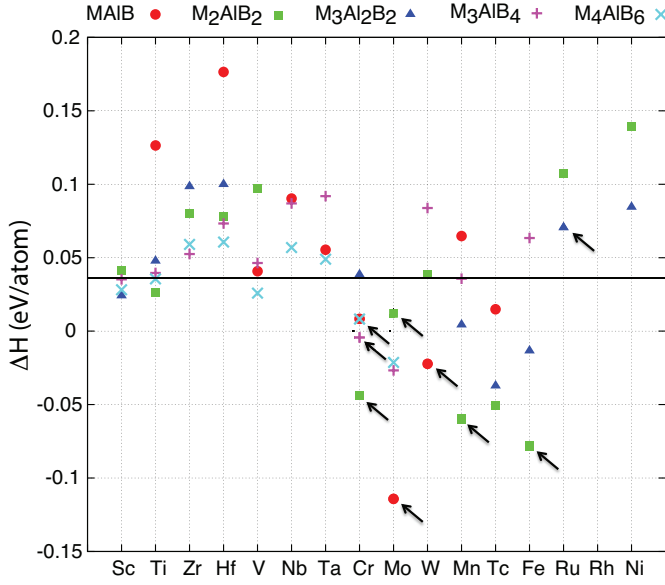


FIG. 2. The relative formation energy ΔH of various MAB phases. The solid black line indicates $\Delta H = 0.036$ eV/atom. The arrows indicate the compounds that have already been synthesized experimentally.

between a pair of adjacent atoms defined as

$$\text{COHP}_{\mu\vec{T},\nu\vec{T}'}(E) = H_{\mu\vec{T},\nu\vec{T}'} \sum_{j,\vec{k}} f_j(\vec{k}) C_{\mu\vec{T},j}^*(\vec{k}) C_{\nu\vec{T}',j}(\vec{k}) \delta(\epsilon_j(\vec{k}) - E), \quad (1)$$

where $H_{\mu\vec{T},\nu\vec{T}'}$ is the matrix element of the Hamiltonian matrix H and $C_{\mu\vec{T},j}(\vec{k})$ represents the eigenvector coefficient of an atomic orbital μ . $\epsilon_j(\vec{k})$ is the j th band energy at momentum \vec{k} , \vec{T} is the translational lattice vector, and $f_j(\vec{k})$ is the occupation number of that state. In analogy to the density of states (DOS), for which the energy integration up to the Fermi energy gives the number of electrons, the energy integration of all COHP for a pair of atoms up to the Fermi energy (ICOHP) can imply the bond strength [61]. All the COHP calculations are performed using the Local Orbital Basis Suite Towards Electronic-Structure Reconstruction (LOBSTER) code [62–64] with the pbeVasFit2015 basis set.[64]

The static exfoliation energy E_{exf} of a bulk MAB phase into 2D MBene is calculated, *e.g.* for the case of $M_2\text{AlB}_2$, through $E_{\text{exf}} = -[E_{\text{tot}}(M_2\text{AlB}_2) - 2E_{\text{tot}}(M_2\text{B}_2) - 2E_{\text{tot}}(\text{Al})] / (4S)$, where $E_{\text{tot}}(M_2\text{AlB}_2)$, $E_{\text{tot}}(M_2\text{B}_2)$ and $E_{\text{tot}}(\text{Al})$ stand for the total energies of bulk $M_2\text{AlB}_2$ phase, 2D $M_2\text{B}_2$ MBene, and Al atom, respectively. The total energy of Al atom, $E_{\text{tot}}(\text{Al})$, is estimated from its bulk structure. Here, S is the surface area of the rectangular lattice, which is simply calculated by multiplication of a and c lattice parameters of the $M_2\text{AlB}_2$ phase. Each unit cell of the $M_2\text{AlB}_2$ phase generates two MBene layers with totally 4 surfaces. Hence, the exfoliation energy is divided by 4 in the above formula. To calculate E_{exf} for other MAB phases, the above formula should be modified appropriately according to the number of Al atoms and the number of MBene layers in the cell.

II. RESULTS AND DISCUSSION

A. Stabilities of MAB phases

In order to find the trends in structural properties of MAB phases, we first investigate the dynamic stabilities of $M\text{AlB}$, $M_2\text{AlB}_2$, $M_3\text{Al}_2\text{B}_2$, $M_3\text{AlB}_4$, and $M_4\text{AlB}_6$ ($M = \text{Sc, Ti, Zr, Hf, V, Nb, Ta, Cr, Mo, W, Mn, Tc, Fe, Ru, Co, Rh, and Ni}$). Table I lists the names and lattice parameters of MAB phases that we found dynamically stable based on the phonon calculations. There is no negative phonon frequency in the phonon spectra for these systems, shown in the supporting information file †. All structures that have already been synthesized experimentally are among the MAB phases that we find stable in Table I. The lattice parameters for the experimentally existing $M\text{AlB}$ ($M = \text{Mo and W}$), $M_2\text{AlB}_2$ ($M = \text{Cr, Mn, and Fe}$), $M_3\text{AlB}_4$, and $M_4\text{AlB}_6$ are in excellent agreement with our theoretical results; the errors are less than 1.5% except for the case of $\text{Ru}_3\text{Al}_2\text{B}_2$ in which the error is around 4.5%. These results indicate the high quality of our calculations.

Next, in order to determine if the dynamically stable MAB phases found above can be realized experimentally, we calculate the formation energy ΔH of the MAB phases with respect to a combination of most competitive phases summarized in Table I; $\Delta H = E_{\text{tot}}(\text{MAB phase}) - E_{\text{tot}}(\text{competitive phases})$, where E_{tot} is the total energy. The most competing phases are found through the open quantum materials database (OQMD).[65, 66] In order to observe the trend better, the ΔH is plotted with respect to transition metals in Figure 2. The negative (positive) ΔH indicates the relative stability (instability) of MAB phases with respect to the competitive phases. The more negative (positive) ΔH indicates the higher (smaller) chance for a synthesis of the MAB phases experimentally. In excellent agreement with experimental observation, some of the Cr-, Mo-, W-, Mn-, and Fe-based MAB phases find negative ΔH (see Figure 2), indicating their synthesis possibility in experiment.[48–50, 53] The negative ΔH of Tc-based MAB phases implies the high chance for their synthesis although there has been no experimental report. This might be due to the lack of experiments on Tc-based MAB phases or there might be some binary Tc–Al or Tc–B, or ternary Tc–Al–B phases that have not been characterized experimentally yet, preventing the formation of Tc-based MAB phases. Further experiments on Tc–Al–B are highly desirable for the discovery of new Tc–Al, Tc–B, or Tc–Al–B phases.

Despite the experimental synthesis of $\text{Ru}_3\text{Al}_2\text{B}_2$,[46] the calculated ΔH is a relatively high positive value (0.07 eV/atom). This might imply that either our exchange-correlation function for Ru is not appropriate or this compound could be formed experimentally because of the influences of vibrational entropy at high temperature and/or boron vacancies entropy effects [67]. According to the recent computational screening on inorganic crystal structure database (ICSD),[68] 20% of all compounds have instability of ΔH larger than 0.036 eV/atom.[69] In such a case, $\text{Ru}_3\text{Al}_2\text{B}_2$ might be one of them. In other words, 80% of experimentally synthesized compounds possess instability of ΔH less

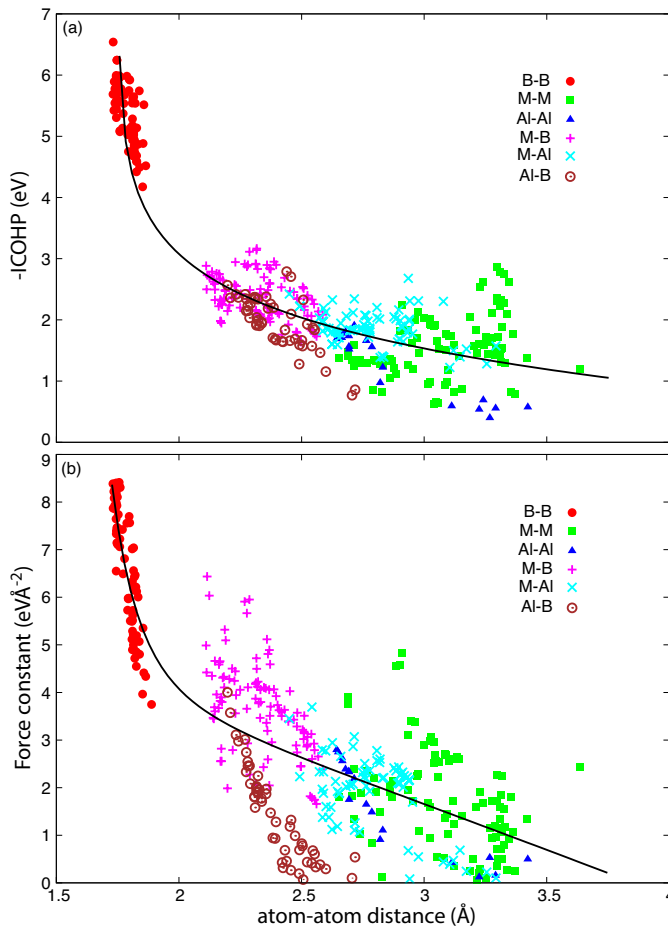


FIG. 3. (a) integrated crystal orbital Hamilton population (ICOHP) and (b) force constants between various atoms in MAB phases. The solid lines are the guides to the eyes.

than 0.036 eV/atom.[69] Assuming this value as a stability criterion (*i.e.*, $\Delta H < 0.036$ eV/atom), it is expected that there is a possibility for the experimental synthesis of Sc-, Ti-, and V-based MAB phases, in addition to Cr-, Mo-, W-, Mn-, Tc-, Fe-, and Ru-based MAB phases. In this study, we have focused on MAB phases with one type of transition metals. However, in the recent computational studies, it has been pointed out that it might be possible to synthesis ordered MAB phases with double transition metals, $M_2M'AIB_4$ ($M = \text{Mn, Fe, Co, M}' = \text{Cr, Mo, W}$). [70]

It is noteworthy that the synthesis of a pure MAB phase instead of multiple phases needs many trials. Experimentalists usually focus on transition metals that do not have many binary M–B or M–Al compounds. Then, one can try to improve the purity of a targeted phase by optimizing the experimental conditions such as temperature, the speed of quenching, and stoichiometry of mixture of transition metals, boron, and aluminum.

B. Bond strength properties of MAB phases

As described above, Al-containing layered materials are of great interest for obtaining novel 2D materials. In this regard, Al-containing MAB phases are a family of promising candidates for realizing 2D transition metal borides. In MAB phases, MoAlB with double layers of Al has partially been etched into 2D MoB by removing Al atoms.[20, 21] Cr_2AlB_2 has also been etched completely into 2D CrB MBene.[22, 23] Current theoretical and experimental knowledge on exfoliation possibility of MAB phases is very limited.

The exfoliation is a dynamic chemical process that depends on the type of etchant, its concentration, the time duration of the treatment, and temperature. Similar to MAX phases, the obtained 2Ds from MAB phases will be covered with a mixture of O, OH, or F during exfoliation due to the chemical reactivity of transition metals.[32, 33] It has been shown that the surface termination can affect the stability of MXenes by forming chemical bonds between the chemical groups and the transition metals.[32, 33] In a similar way, it is expected the surface termination can affect the stability of MBene too. If one aims to simulate the exfoliation process using molecular dynamics simulations by including all above details, it will be very difficult and time-consuming and will almost be impossible to compare the exfoliation processes of different compounds or phases together. Therefore, the static calculations are almost the only efficient way to investigate or extract useful information about exfoliation possibility of layered materials. Here, a set of static calculations are used to examine the bond strength properties to systematically study the exfoliation possibility of MAB phases. This is because in a successful chemical process, the bond between an Al atom and its neighboring Al, M, and B atoms should be broken without destroying the other bonds. The weaker the M–Al bonds are, the higher the exfoliation possibility becomes. It is noteworthy that in our previous study,[9] we successfully applied the same analysis on MAX phases. We predicted 37 new MAX phases that could be exfoliated. Later on, it was experimentally shown that Ti_3SiC_2 , one of the phases that we also predicted, could be exfoliated into Ti_3C_2 . [71]

The strength of a bond in a material can be approximately measured on the basis of the integrated COHP (ICOHP) analyses and the force constant calculations. The ICOHP has already been used to measure the bond strength in various materials.[62–64] Previously, the force constants were used to measure the strength of bonds in diatomic dimers, molecules and clusters.[72–75] Recently, it has been expanded to study bond strengths in solids [9, 59, 76, 77] and interfaces.[78, 79] We have also applied these two methods on MAX phase family. We have shown that generally, M–Al bonds in MAX phases are weaker than M–X bonds, which implies that M–Al bonds are relatively easily broken in MAX phases during the exfoliation process.[9] However, it should be noted that neither of ICOHP nor force constant can perfectly describe the bond strength; the ICOHP mainly measures the strength of the covalency of a bond, but not its ionicity, while the force constant describes the behavior of energy potential when the bond is slightly stretched from its equilibrium size, but not its

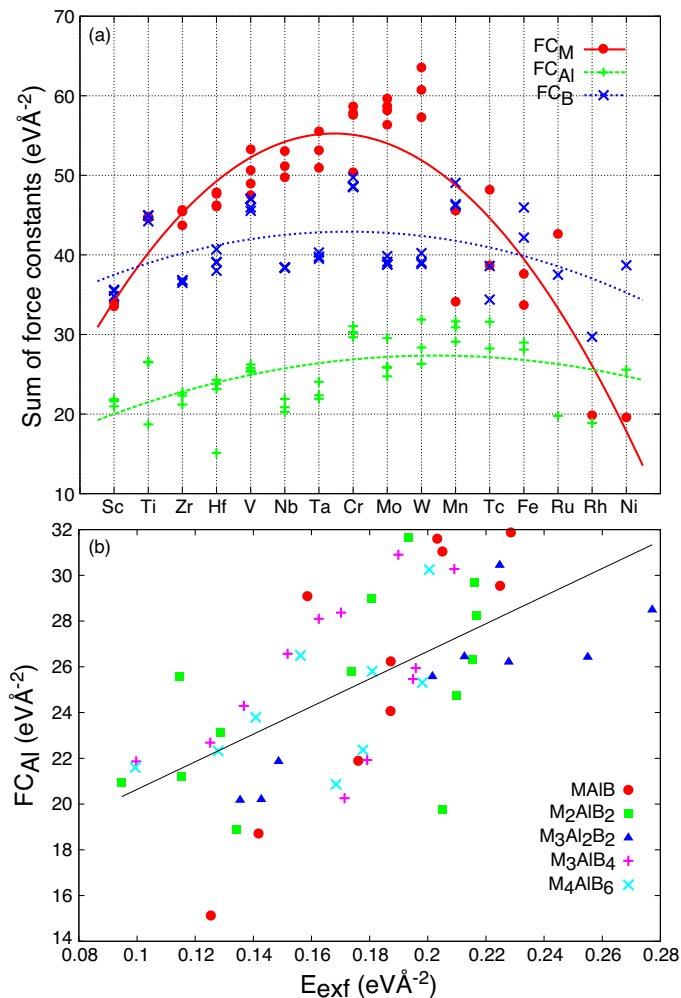


FIG. 4. (a) The sum of the force constants for all bonds connected to an M, Al, and B atoms of various MAB phases. The lines are the guides to the eyes. (b) FC_{Al} versus the static exfoliation energy (E_{exf}) for various MAB phases. The correlation coefficient of the fitted line is $r = 0.622$.

dissociation state.[9]

Figure 3 summarizes the results of ICOHP and force constant calculations for various M–B, M–Al, M–M, Al–Al, Al–B, and B–B bonds in MAB phases. The results of both quantities show almost the same trends. Generally, as the atom–atom distance increases, the bond strength decreases. As shown in Fig. 3, in general, the B–B and M–B bonds are stiffer than the M–Al, M–M, Al–Al, and Al–B bonds. This is consistent with the recent investigation on mechanical response of MoAlB and WAlB to external strain, finding that the cleavage occurs along the Al–Al layers due to the weak Al–Al bonds.[80] It is noteworthy that exceptionally the Ni–Al is stiffer than Ni–B. The B–B, M–B, and M–M bonds are the ones that construct the MB, M_2B_3 , and M_3B_4 block units in MAB phases and are stronger than the M–Al, Al–Al, and Al–B bonds, implying the possibility of exfoliation of MAB phases by breaking the bonds between Al atoms and neighboring M, Al, and B atoms without hurting the 2D

MB, M_2B_3 , and M_3B_4 backbones, *i.e.*, MBenes. In MAX phases, the strong M–X ($X = \text{C}$ or N) bonds construct the backbones, *i.e.*, $M_{n+1}X_n$ MXenes. Our calculations indicate the B–B bonds in MAB phases are as strong as the M–X ($X = \text{C}$ or N) bonds in MAX phases.[9] This can be a sign that 2D MB, M_2B_3 , and M_3B_4 may remain stable after the exfoliation process as in the case of $M_{n+1}X_n$ MXenes. The data in Figs. 3(a) and (b) are shown for each phase separately in the supporting information file †.

C. Exfoliation possibility of MAB phases into 2D MBenes

In order to better understand the exfoliation possibility of MAB phases, we also calculate the sum of the force constants for all bonds connected to individual M, Al, or B atom (listed as FC_M , FC_{Al} , or FC_B in Table I) and the results are shown in Fig. 4(a) with respect to the transition metals in various MAB phases. The FC_M and FC_B are calculated for the M and B atoms that are closest to the Al atom. The larger the FC_M and FC_B are, the higher the chance is for obtaining perfect 2D MB, M_2B_3 , and M_3B_4 after the exfoliation process. The smaller FC_{Al} indicates the ease for the breaking the bonds between an Al atom with its all neighboring atoms. We have investigated the change of FC_{Al} as a function of static exfoliation energy, shown in Fig. 4(b). As seen from this figure, the smaller (larger) FC_{Al} appears to relate linearly with the smaller (larger) E_{exf} in each phase, although the linear correlation in $M_2\text{AlB}_2$ seems relatively lower than that in the other phases. A guideline of the overall trend between FC_{Al} and E_{exf} is shown in Fig. 4(b) with the linear correlation coefficient of 0.622. This positive correlation can help us to explore exfoliation possibilities in an early study of the MAB materials. The data in Figs. 4(a) and (b) are shown for each phase separately in the supporting information file †.

As shown in Fig. 4(a), in most of MAB phases, $FC_M > FC_B > FC_{Al}$. We also find that FC_M , FC_B , and FC_{Al} continuously increase when the type of transition metal changes from Sc→W, while FC_M and FC_B start decreasing when the transition metal is changed from W→Ni. The family of Cr-, Mo-, and W-based MAB phases obtain almost the highest FC_M and FC_B , implying that these MAB phases may have large elastic constants and there will be a good chance for obtaining perfect 2D MB, M_2B_3 , and M_3B_4 MBenes. In Mn→Ni MAB phases, the FC_M , FC_B , and FC_{Al} start decreasing. Therefore, there is a less chance to obtain perfect MBenes in these MAB phases because the etchant can wash out not only the Al atoms but also M and B atoms. Our calculations predict that when the transition metal changes from Sc→W (Mn→Ni), the degree of mechanical anisotropy of MAB phases increases (decreases).

Experimentally, MoAlB with double layers of Al atoms has been partially etched into 2D MoB MBene[20, 21] and Cr_2AlB_2 has also been etched completely into 2D CrB MBene.[22, 23] In the family of Cr-, Mo-, and W-based MAB phases, we find in Fig. 4(a) that the bonding between Al atoms and other atoms are very strong. Indeed, the total force constant FC_{Al} for MoAlB is $29.542 \text{ eV}\text{\AA}^{-2}$ (see Table I). This implies that if experimentalists were able to exfoliate MoAlB

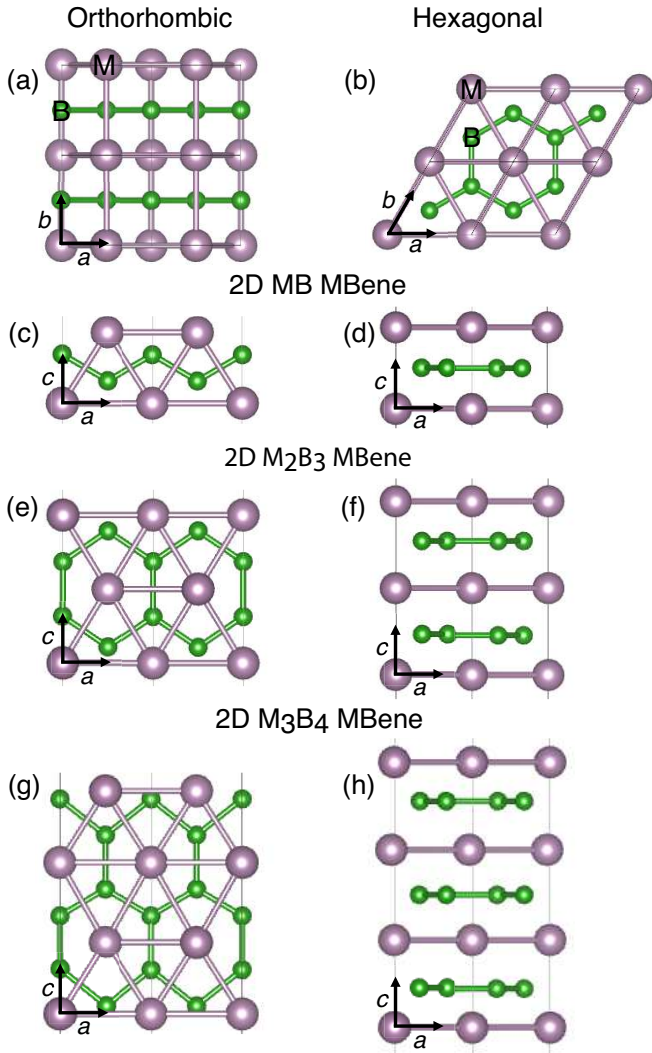


FIG. 5. Top views of (a) rectangular and (b) hexagonal 2D MB, M_2B_3 , and M_3B_4 MBenes. (c), (e), and (g) [(d), (f), and (h)] Side views of rectangular (hexagonal) 2D MB, M_2B_3 , and M_3B_4 , respectively. a , b , and c directions are indicated by arrows. The structures are periodic in ab plane and vacuum space of 30 Å exists along the c axis.

partially, the full or partial exfoliation of all MAB phases from Sc→W might also be possible. This is consistent with the experimental results that experimentalists succeeded to exfoliate Cr_2AlB_2 into 2D CrB nanosheets.[22, 23]

Unfortunately, the experimental data on the exfoliation of MAB phases is still very limited. However, there are many on the exfoliation of MAX phases. By investigating MAX phases, we have found previously that MAX phases already exfoliated into 2D MXenes satisfy $FC_M > 44.253$, $FC_{Al} < 21.855$, FC_X ($X = C$ or N) > 40.511 eV/Å². [9] By comparing the FC_{Al} values of MAB phases with those of the exfoliated MAX phases, we find that the FC_{Al} values in MAB phases are larger than those in MAX phases. This suggests that the exfoliation of MAB phases is more difficult than MAX phases and explains why MoAlB was not completely exfoliated experi-

mentally. As a strategy to enhance the exfoliation possibility of MoAlB, it might be appropriate to alloy MoAlB with other transition metals, *e.g.*, $M' = Sc, Ti, Zr, Hf, V, Nb,$ or Ta in which their corresponding MAB phases possess lower FC_{Al} values. In this way, removing Al atoms from $Mo_xM'_{1-x}AlB$ phase might become easier.

Our force constant data in Fig. 4(a) indicate that depending on the transition metal, some of the phases possess the FC_{Al} of almost in the same range, therefore all those phases may have similar chances for Al removal. However, as explained before, the perfectness of the obtained 2D MBenes will depend on FC_M and FC_B .

D. Structural phase transformation of 2D MBenes

In 2D $M_{n+1}X_n$ MXenes, it has been observed experimentally that upon heating, the 2D MXenes transform into nanocrystals of transition metal oxides and disordered graphitic carbon structures.[81] It is also known that some of the transition metals, $M = Sc, Ti, V, Nb, Ta, Cr, Mo,$ and W , have MB_2 hexagonal structures.[82] Therefore, it might be plausible that orthorhombic 2D MB, M_3B_4 , and M_2B_3 MBenes with rectangular lattice structures transform into monolayer or multilayers of graphene-like boron sheets sandwiched between transition metals, as shown in Fig. 5. The orthorhombic 2D MB, M_3B_4 , and M_2B_3 contain zigzag single, double, or triple chains of boron atoms, respectively. In M_3B_4 and M_2B_3 , the zigzag chains form strips of boron hexagonal networks. During the transformation from rectangular lattice to a hexagonal lattice, the zigzag chains start bonding to each other on ab plane, and consequently the chains or hexagonal strips transform into single, double, and triple graphene-like boron sheets shown in Fig. 5. In order to determine which of the 2D MBenes with orthorhombic or hexagonal lattices are preferable for a particular application, additional calculations will be necessary.

Here, we calculate the energy barrier for such a transformation for the 2D MB MBenes from the orthorhombic to a hexagonal phase using nudged elastic band (NEB) method.[83, 84]. The results are shown in Fig. 6. We find that the 2D MB ($M = Sc, Ti, Zr, Hf, V, Nb, Ta, Mo,$ and W) MBenes with hexagonal lattice structures are more stable than the orthorhombic phases. In contrast, we find that the orthorhombic phases are more stable for $M = Cr, Mn, Tc, Fe, Ru,$ and Ni . This is reasonable because $Sc, Ti, Zr, Hf, V, Nb, Ta, Mo,$ and W are found experimentally to form in hexagonal binary boride phases.[82] Our NEB calculations indicate that the energy barrier for transformation from the orthorhombic to hexagonal phase is between 0.2–0.4 eV/atom. However, it should be noted that this energy barrier is overestimated because it is very difficult to consider the possibility of nucleation of the boron sheets in our calculations.

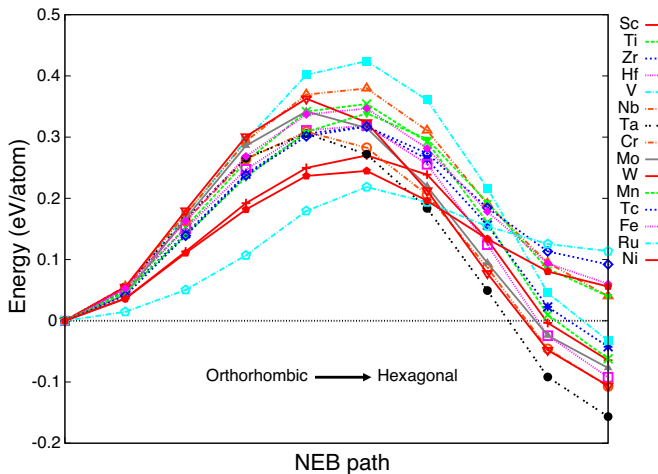


FIG. 6. The energy barrier for structural transformation of 2D MBenes from the rectangular lattice to hexagonal lattice structures calculated using the nudged elastic band (NEB) method.

III. CONCLUSION

Recently, a layered family of Al-containing transition metal borides, known as MAB phases has received attention for obtaining 2D transition metal borides, *i.e.*, 2D MB, M_2B_3 , and M_3B_4 MBenes. Currently, there exist only a few members of MAB phases, mainly made of Cr, Mo, W, Mn, and Fe. Here, based on the phonon and formation energy calculations, we have shown that in addition to these MAB phases, Sc, Ti,

V, and Tc-based MAB phases are also possible to be realized. The bond strength analyses indicate the B–B and M–B bonds are stronger than M–Al, Al–B, and Al–Al bonds, implying the successful exfoliation possibility of MAB phases into 2D MBenes. Our analyses indicate that Cr-, Mo-, and W-based MAB phases are the best candidates for obtaining 2D MBenes. To enhance the exfoliation possibility of Cr-, Mo-, and W-based MAB phases, we suggest to alloy these MAB phases with Sc, Ti, Zr, Hf, V, Nb, or Ta. Furthermore, we have investigated the structural transformation of 2D MBenes from the orthorhombic to hexagonal phase, which results in the formation of graphene-like boron sheets sandwiched between transition metals. This transformation might be possible at high temperatures especially for the case of Sc-, Ti, Zr-, Hf-, V-, Nb-, Ta-, Mo-, and W-based MBenes.

CONFLICTS OF INTEREST

There are no conflicts to declare.

ACKNOWLEDGEMENTS

M.K. is grateful to RIKEN Advanced Center for Computing and Communication (ACCC) for the allocation of computational resource of the RIKEN supercomputer system (HOKUSAI GreatWave). Part of the calculations were also performed on Numerical Materials Simulator at National Institute for Materials Science (NIMS). M.K. gratefully acknowledges the support by Grant-in-Aid for Scientific Research (No. 17K14804) from MEXT Japan.

-
- [1] M. W. Barsoum, *Prog. Solid State Chem.*, 2000, **28**, 201–281.
- [2] M. Khazaei, M. Arai, T. Sasaki, M. Estili and Y. Sakka, *J. Phys.: Condens. Matter*, 2014, **26**, 505503.
- [3] M. Ashton, R. G. Hennig, S. R. Broderick, K. Rajan and S. B. Sinnott, *Phys. Rev. B*, 2016, **94**, 054116.
- [4] M. Naguib, M. Kurtoglu, V. Presser, J. Lu, J. Niu, M. Heon, L. Hultman, Y. Gogotsi and M. W. Barsoum, *Adv. Mater.*, 2011, **23**, 4248–4253.
- [5] M. Naguib, O. Mashtalir, J. Carle, V. Presser, J. Lu, L. Hultman, Y. Gogotsi and M. W. Barsoum, *ACS Nano*, 2012, **6**, 1322–1331.
- [6] B. Anasori, M. Dahlqvist, J. Halim, E. J. Moon, J. Lu, B. C. Hosler, E. N. Caspi, S. J. May, L. Hultman, P. Eklund, J. Rosén and M. W. Barsoum, *J. Appl. Phys.*, 2015, **118**, 94304.
- [7] R. Meshkian, Q. Tao, M. Dahlqvist, J. Lu, L. Hultman and J. Rosen, *Acta Mater.*, 2017, **125**, 476–480.
- [8] M. Dahlqvist, A. Petruhins, J. Lu, L. Hultman, and J. Rosen, *ACS Nano*, 2018, **12**, 7761–7770.
- [9] M. Khazaei, A. Ranjbar, K. Esfarjani, D. Bogdanovski, R. Dronskowski, Y. Yunoki, *Phys. Chem. Chem. Phys.*, 2018, **20**, 8579–8592.
- [10] M. Naguib, J. Halim, J. Lu, K. M. Cook, L. Hultman, Y. Gogotsi, M. W. Barsoum, *J. Am. Chem. Soc.*, 2013, **135**, 15966–15969.
- [11] M. Ghidui, M. Naguib, C. Shi, O. Mashtalir, L. M. Pan, B. Zhang, J. Yang, Y. Gogotsi, S. J. L. Billinge, M. W. Barsoum, *Chem. Commun.*, 2014, **50**, 9517–9520.
- [12] P. Urbankowski, B. Anasori, T. Makaryan, D. Er, S. Kota, P. L. Walsh, M. Zhao, V. B. Shenoy, M. W. Barsoum, Y. Gogotsi, *Nanoscale*, 2016, **8**, 11385–11391.
- [13] B. Soundiraraju, B. K. George, *ACS Nano*, 2017, **11**, 8892–8900.
- [14] M. Alhabeab, K. Maleski, T. S. Mathis, A. Sarycheva, C. B. Hatter, S. Uzun, A. Levitt, and Y. Gogotsi, *Angew. Chem. Int. Ed. Engl.*, 2018, **57**, 5444–5448.
- [15] M. H. Tran, T. Schäfer, A. Shahraei, M. Dürschnabel, L. Molina-Luna, U. I. Kramm, C. S. Birkel, *ACS Appl. Energy Mater.*, 2018, **1**, 3908–3914.
- [16] R. Meshkini, L. -Å. Näslund and J. Halim, *Scr. Mater.*, 2015, **108**, 147–150.
- [17] J. Zhou, X. Zha, F. Y. Chen, Q. Ye, P. Eklund, S. Du, Q. Huang, *Angew. Chem. -Int. Edit.*, 2016, **55** 5008–5013.
- [18] J. Zhou, X. Zha, X. Zhou, F. Chen, G. Gao, S. Wang, C. Shen, T. Chen, C. Zhi, P. Eklund, S. Du, J. Xue, W. Shi, Z. Chai, and Q. Huang, *ACS Nano*, 2017, **11**, 3841–3850.
- [19] J. Zhou, X. -H. Zha, M. Yildizhan, P. Eklund, J. Xue, M. Liao, P. O. Å. Persson, S. Du, and Q. Huang, *ACS Nano*, 2019, **13**, 1195–1203.

- [20] L. T. Alameda, C. F. Holder, J. L. Fenton, and R. E. Schaak, *Chem. Mater.*, 2017, **29**, 21, 8953–8957.
- [21] L. T. Alameda, P. Moradifar, Z. P. Metzger, N. Alem, and R. E. Schaak, *J. Am. Chem. Soc.*, 2018, **140**, 8833–8840.
- [22] H. Zhang, H. Xiang, F. -Z. Dai, Z. Zhang, and Y. Zhou, *J. Mater. Sci. Technol.*, 2018, **34**, 2022–2026.
- [23] H. Zhang, F. -z. Dai, H. Xiang, X. Wang, Z. Zhang, and Y. Zhou, *J. Mater. Sci. Technol.*, 2019, <https://doi.org/10.1016/j.jmst.2019.03.031>.
- [24] J. Wang, M. Khazaei, M. Arai, N. Umezawa, T. Tada, and H. Hosono, *Chem. Mater.*, 2017, **29**, 5922–5930.
- [25] J. Yu, M. Khazaei, N. Umezawa, and J. Wang, *J. Mater. Chem. C*, 2018, **6**, 5803–5811.
- [26] Y. Shao, M. Shao, Y. Kawazoe, X. Shi, and H. Pan, *J. Mater. Chem. A*, 2018, **6**, 10226–10232.
- [27] G. Yuan, T. Bo, X. Qi, P. -F. Liu, Z. Huang, B. -T. Wang, *Appl. Surf. Sci.*, 2019, **480**, 448–453.
- [28] B. Zhang, L. Fan, J. Hu, J. Gu, B. Wang, and Q. Zhang, *Nanoscale*, 2019, **11**, 7857–7865.
- [29] Z. Guo, J. Zhou, and Z. Sun, *J. Mater. Chem. A*, 2017, **5**, 23530–23535.
- [30] T. Bo, P. -F. Liu, J. Zhang, F. Wang, and B. -T. Wang, *Phys. Chem. Chem. Phys.*, 2019, **21**, 5178–5188.
- [31] Z. Jiang, P. Wang, X. Jiang, and J. Zhao, *Nanoscale Horiz.*, 2018, **3**, 335–341.
- [32] M. Khazaei, A. Ranjbar, M. Arai, T. Sasaki, S. Yunoki, *J. Mater. Chem. C*, 2017, **5**, 2488–2503.
- [33] M. Khazaei, A. Mishra, N. S. Venkataramanan, A. K. Sing, *Curr. Opin. Solid State Mater. Sci.* 2019, DOI: <https://doi.org/10.1016/j.cossms.2019.01.002>.
- [34] B. Anasori, M. R. Lukatskaya, Y. Gogotsi, *Nat. Rev.*, 2017, **2**, 16098.
- [35] B.-M. Jun, S. Kim, J. Heo, C. M. Park, N. Her, M. Jang, Y. Huang, J. Han, Y. Yoon, *Nano Res.*, 2018, **12**, 471.
- [36] J. Pang, R. G. Mendes, A. Bachmatiuk, L. Zhao, H. Q. Ta, T. Gemming, H. Liu, Z. Liu, Mark H. Rummeli, *Chem. Rev. Soc.*, 2019, **48**, 72–133.
- [37] A. L. Ivanovskii and A. N. Enyashin, *Russ. Chem. Rev.*, 2013, **82**, 735.
- [38] N. K. Chaudhari, H. Jin, B. Kim, D. S. Baek, S. H. Joo, K. Lee, *J. Mater. Chem. A*, 2017, **5**, 24564–24579.
- [39] J. Zhu, E. Ha, G. Zhao, Y. Zhou, D. Huang, G. Yue, L. Hu, N. Sun, Y. Wang, L. Y. S. Lee, C. Xu, K.-Y. Wong, D. Astruc, and P. Zhao, *Coord. Chem. Rev.*, 2017, **352**, 306–327.
- [40] H. Wang, Y. Wu, X. Yuan, G. Zeng, J. Zhou, X. Wang, J. W. Chew, *Adv. Mater.*, 2018, **30**, 1704561.
- [41] X. Li, C. Wang, Y. Cao, G. Wang, *Chem. Asian J.*, 2018, **13**, 2742–2752.
- [42] X. Zhang, Z. Zhang, and Z. Zhou, *J. Energy Chem.*, 2018, **27**, 73–85.
- [43] Y. Zhang, L. Wang, N. Zhang, Z. Zhou, *RSC Adv.*, 2018, **8**, 19895–19905.
- [44] K. Hantanasirisakul and Y. Gogotsi, *Adv. Mater.*, 2018, **30**, 1804779.
- [45] H. Lin, Y. Chen, and J. Shi, *Adv. Sci.*, 2018, **5**, 1800518.
- [46] W. Jung and K. Schweitzer, Z. Kristallogr. Kristallgeom. Kristallphys. Kristallchem. 1986, **174**, 109–110.
- [47] X. Tan, P. Chai, C. M. Thompson and M. Shatruk, *J. Am. Chem. Soc.*, 2013, **135**, 9553–9557.
- [48] M. Ade and H. Hillebrecht, *Inorg. Chem.*, 2015, **54**, 6122–6135.
- [49] P. Chai, S. A. Stoian, X. Tan, P. A. Dube, and M. Shatruk, *J. Solid State Chem.*, 2015, 224, 52–61.
- [50] S. Kota, E. Zapata-Solvas, A. Ly, J. Lu, O. Elkassabany, A. Huon, W. E. Lee, L. Hultman, S. J. May, and M. W. Barsoum *Sci. Rep.*, 2016, **6**, 26475.
- [51] J. Lu, S. Kota, M. W. Barsoum and L. Hultman, *Mater. Res. Lett.*, 2017, **5**, 235–241.
- [52] S. Kota, M. Agne, E. Zapata-Solvas, O. Dezellus, D. Lopez, B. Gardiola, M. Radovic and M. W. Barsoum, *Phys. Rev. B*, 2017, **95**, 144108.
- [53] T. N. Lamichhane, L. Xiang, Q. Lin, T. Pandey, D. S. Parker, T. -H. Kim, L. Zhou, M. J. Kramer, S. L. Bud'ko, and P. C. Canfield, *Phys. Rev. Materials*, 2018, **2**, 084408.
- [54] G. Kresse and J. Furthmüller, *Comput. Mater. Sci.*, 1996, **6**, 15–50.
- [55] J. P. Perdew, K. Burke and M. Ernzerhof, *Phys. Rev. Lett.*, 1996, **77**, 3865.
- [56] H. J. Monkhorst and J. D. Pack, *Phys. Rev. B*, 1976, **13**, 5188.
- [57] A. Togo, F. Oba and I. Tanaka, *Phys. Rev. B*, 2008, **78**, 134106.
- [58] A. J. E. Foreman and W. M. Lomer, *Proc. Phys. Soc. London, Sect. B*, 1957, **70**, 1143.
- [59] Y. Liu, K. T. E. Chua, T. C. Sum, C. K. Gan, *Phys. Chem. Chem. Phys.*, 2014, **16**, 345–350.
- [60] R. Dronskowski and P. E. Blöchl, *J. Phys. Chem.*, 1993, **97**, 8617–8624.
- [61] M. Küpers, P. M. Konze, S. Maintz, S. Steinberg and A. M. Mio, Cojocarú-Miredin, O.; Zhu, M.; Müller, M.; Luysberg, M.; Mayer, J.; Wuttig, M.; Dronskowski, R. *Angew. Chem. Int. Ed.*, 2017, **56**, 10204–1028.
- [62] V. L. Deringer, A. L. Tchougréeff and R. Dronskowski, *J. Phys. Chem. A*, 2011, **115**, 5461–5466.
- [63] S. Maintz, V. L. Deringer, A. L. Tchougréeff, R. Dronskowski, *J. Comput. Chem.*, 2013, **34**, 2557–2567.
- [64] S. Maintz, V. L. Deringer, A. L. Tchougréeff and R. Dronskowski, *J. Comput. Chem.*, 2016, **37**, 1030–1035.
- [65] A. R. Akbarzadeh, V. Ozolinš, and C. Wolverton, *Adv. Mater.*, 2007, **19**, 3233–3239.
- [66] S. Kirklin, B. Meredig, and C. Wolverton, *Adv. Energy Mater.*, 2013, **3**, 252–262.
- [67] M. Dahlqvist, U. Jansson, J. Rosen, *J. Phys.: Condens. Matter*, 2015, **27**, 435702.
- [68] G. Bergerhoff, R. Hundt, and R. Sievers, *J. Chem. Inf. Comput. Sci.*, 1983, **23**, 66–69.
- [69] Y. Wu, P. Lazic, G. Hautier, K. Persson, and G. Ceder, *Energy Environ. Sci.*, 2013, **6**, 157–168.
- [70] F. -Z. Dai, H. Xiang, Y. Sun, and Y. Zhou, *J. Mater. Sci. Technol.*, 2019, DOI: <https://doi.org/10.1016/j.jmst.2019.03.005>.
- [71] M. Alhabeab, K. Maleski, T. S. Mathis, A. Sarycheva, C. B. Hatter, S. Uzun, A. Levitt, and Y. Gogotsi, *Angew. Chem. Int. Ed.* 2018, **57**, 5444–5448.
- [72] R. G. Pearson, *J. Molecular. Struc.*, 1993, **300**, 519–525.
- [73] J. R. Lombardi and B. Davis, *Chem. Rev.*, 2002, **102**, 2431–2460.
- [74] K. Brandhorst and J. Grunenberg, *Chem. Soc. Rev.*, 2008, **37**, 1558–1567.
- [75] D. Cremer and E. Kraka, *Curr. Org. Chem.*, 2010, **14**, 1524–1560.
- [76] V. L. Deringer, R. P. Stoffel, M. Wuttig and R. Dronskowski, *Chem. Sci.*, 2015, **6**, 5255–5262.
- [77] J. Hong and O. Delaire, *arXiv: 1604.07077v2 [cond-mat.mtrl-sci]*, 2016.
- [78] O. V. Pupyshva, A. A. Farajian, C. R. Knick, A. Zhamu and B. Z. Jang, *J. Phys. Chem. C*, 2010, **114**, 21083–21087.
- [79] L. Wang, X. Zhou, T. Ma, D. Liu, L. Gao, X. Li, J. Zhang, Y. Hu, H. Wang, Y. Dai and J. Luo, *Nanoscale*, 2017, **9**, 10846–10853.

- [80] F. Z. Dai, Z. Feng, Y. Zhou, *Comput. Mater. Sci.*, 2018, **147**, 331.
- [81] M. Naguib, O. Mashtalir, M. R. Lukatskaya, B. Dyatkin, C. Zhang, V. Presser, Y. Gogotsi, M. W. Barsoum, *Chem. Commu.*, 2014, **50**, 7420.
- [82] G. Akopov, M. T. Yeung, R. B. Kaner, *Adv. Mater.*, 2017, **29**, 1604506.
- [83] G. Henkelman and H. Jónsson, *J. Chem. Phys.*, 2000, **113**, 9901–9904.
- [84] G. Henkelman and H. Jónsson, *J. Chem. Phys.*, 2000, **113**, 9978–9985.